Earth and Planetary Science Letters 584 (2022) 117505

Contents lists available at ScienceDirect

Earth and Planetary Science Letters

www.elsevier.com/locate/epsl

Decadal change of the Apulia microplate motion preceding the M_W 6.4, 26 November 2019 Durrës (Albania) earthquake

Giampiero Iaffaldano *, Juan Martin de Blas, Bjartur Í Dali Udbø

Department of Geosciences and Natural Resource Management, University of Copenhagen, Denmark

ARTICLE INFO

Article history:
Received 11 October 2021
Received in revised form 4 March 2022
Accepted 15 March 2022
Available online xxxx
Editor: R. Bendick

Dataset link: earthquake.usgs.gov/earthquakes/eventpage/us70006d0m/moment-tensor

Dataset link: cnt.rm.ingv.it/en/event/23487611/?tab=MeccanismoFocale

Dataset link: geofon.gfz-potsdam.de/old/data/alerts/2019/gfz2019xdig/mt.txt

Dataset link: www.globalcmt.org/CMTsearch.html

Keywords:
GPS plate motions
microplate dynamics
interseismic stress

ABSTRACT

It is commonly assumed that the motions of tectonic plates remain steady over the earthquake cycle. This assumption is based on the notion that stresses associated with the cycle may not be sufficient to overcome the asthenosphere viscous resistance at the lithosphere base, which counters plate-motion changes. However, this remains to be verified. Recent inferences on the asthenosphere viscosity/thickness from modelling of glacial rebound data constrain the amount of viscous resistance needed to alter plate motions. In light of these recent findings, it is conceivable that stresses associated with the earthquake cycle are large enough to impact motions of microplates or small-/medium-sized plates. Here we show that the contemporary motion of the Apulia microplate slowed down by $\sim 20\%$ and turned westward by $\sim 10^{\circ}$ during the decade preceding the M_W 6.4, 26 November 2019 Durrës (Albania) earthquake, which struck the Apulia eastern margin with the Eurasia plate. We make a statistical comparison between estimates of the torque variation required for Apulia to generate the observed slowdown, and parameterised estimates of the torque variation imparted to Apulia by the interseismic stress buildup during the decade before the 2019 Durrës earthquake. We conclude that the Apulia motion change likely resulted from the interseismic stress buildup associated with the Durrës earthquake cycle.

1. Introduction

The occurrence of large earthquakes along brittle plate margins is classically studied in the context of the theory of plate tectonics (Wilson, 1965; McKenzie and Parker, 1967; Morgan, 1968; Le Pichon, 1968): over decades to centuries, relative motions between adjacent tectonic plates accrue stress at slow pace along portions of their brittle interfaces – this is referred to as the interseismic stress buildup. Stress is then suddenly released through earthquakes, and the process of stress accrual is thus reset. The whole temporal pattern of slow stress accrual and sudden release is commonly referred to as the earthquake cycle – although such a definition does not necessarily imply that the process repeats itself in the same place and/or with the same period. One of the tenets of the plate tectonics theory is the steadiness of plate motions over the earthquake cycle (e.g., Govers et al., 2018). This forms the basis, for instance, of slip deficit estimates that often inform seismic hazard models (e.g., Savage, 1983). Such a tenet, which remains to be tested against observations, is predicated on the notion that stresses associated with the earthquake cycle (see Allmann and Shearer, 2009, for a review) appear small relative to what is needed to overcome viscous resistance at the plates base and change plate motions over time (e.g., Iaffaldano, 2014). While this notion appears reasonable for large tectonic plates, medium to small plates as well as microplates (Wallace et al., 2005) offer a relatively smaller area to viscous resistance from the underlying asthenosphere. Their motions, therefore, might be more prone to be influenced by relatively small stress changes along their tectonic margins. In addition to this, recent advances in modelling of long-wavelength glacial rebound data place tighter constraints on thickness and viscosity of the Earth's asthenosphere (Paulson and Richards, 2009; Richards and Lenardic, 2018): these analyses indicate that the cube of the asthenosphere thickness is proportional to the viscosity contrast between the asthenosphere and the upper part of the mantle. This finding has bearing on analyses of the plate torque balance, because the interdependence of thick-

* Corresponding author.
E-mail address: giia@ign.ku.dk (G. Iaffaldano).

https://doi.org/10.1016/j.epsl.2022.117505

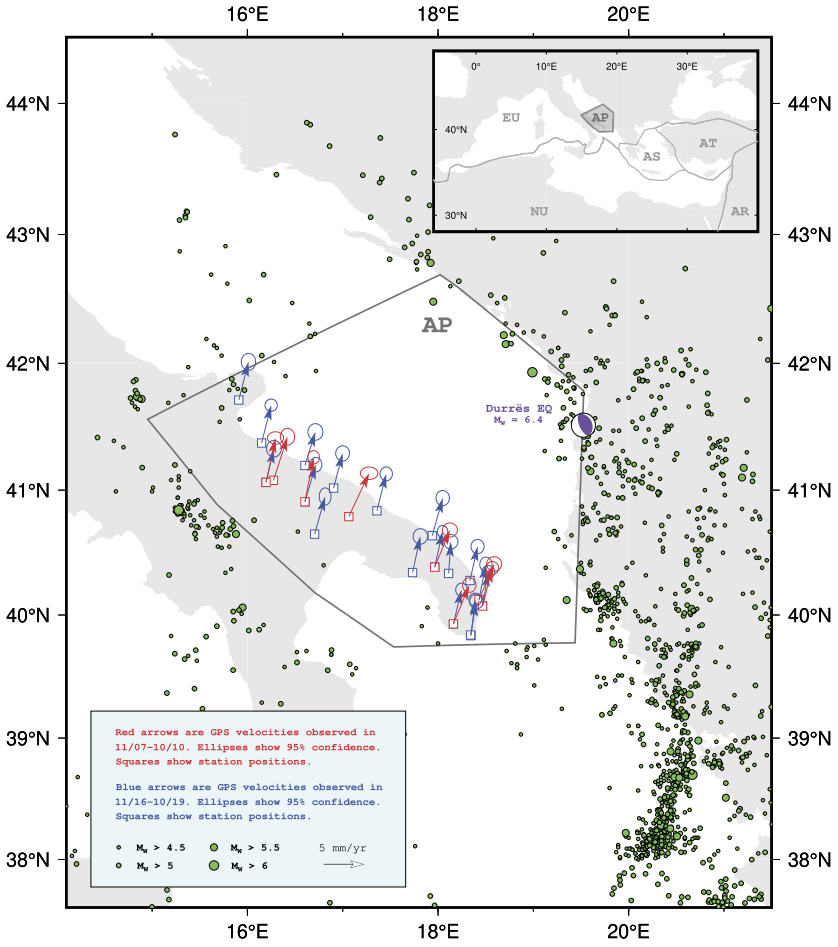

Fig. 1. GPS surface velocities utilised in this study to infer Euler vectors for the Apulia (AP) rigid motion during the periods from November 2007 to December 2010 (in red), and from November 2016 to October 2019 (in blue). Squares are GPS-site locations. Ellipses show the 95% confidence on GPS velocities. Green dots are historical and instrumentally-detected earthquakes from the SHEEC 1900–2006 Catalog and the European-Mediterranean Regional Centroid-Moment Tensors Catalog. In purple is the epicentre and focal mechanism (USGS solution) of the M_W 6.4 November 2019 Durrës earthquake. AP microplate margins are in black. Continents are in grey. Inset shows the location of AP within the Mediterranean tectonic setting – AT is Anatolia, AR is Arabia, AS is Aegean Sea, EU is Eurasia, and NU is Nubia. (For interpretation of the colours in the figure(s), the reader is referred to the web version of this article.)

ness and viscosity of the asthenosphere reduces significantly the ranges of torque values required to modify plate motions through time (e.g., Stotz et al., 2018). Taken altogether, these findings mean that small tectonic plates or microplates require relatively moderate levels of torque to change their motions. This opens to the possibility that they might experience temporal motion changes associated with the stress buildup and release of the earthquake cycle. In fact, from the viewpoint of plate dynamics, the whole earthquake cycle can in principle be thought as comprising two phases in which two torques are built upon a plate: a first phase in which a plate experiences a torque whose magnitude slowly grows as the stress builds up along a portion of its margins during the interseismic period. In the subsequent phase, corresponding to the earthquake itself, the plate experiences a sudden, additional torque that is equal in magnitude (at least to first-degree) but opposite in direction to the one developed during the first phase. This way, the net torque change upon the plate from the beginning to the end of the earthquake cycle remains null. It follows from this that one should expect differences in plate motions when these are measured at different moments within a single earthquake cycle, but that the average motion throughout one or more complete cycles should be expected to be steady. The hypothesis that the motions of small plates and microplates are influenced by the stress evolution over the earthquake cycle is indeed supported by synthetic numerical models of microplate kinematics and dynamics (Martin de Blas and Iaffaldano, 2019), but remains to be tested against real data.

The Mediterranean tectonic setting is a prime example of microplates that buffer the relative motions between major tectonic plates (Faccenna et al., 2014). In fact, from East to West convergence between Nubia and Eurasia is accommodated through the motions of microplates and units such as Anatolia, the Aegean Sea, Apulia, Adria, and the Eastern Mediterreanean (e.g., Jolivet and Faccenna, 2000; Nocquet, 2012). Consequently, this is a region of significant seismic activity that is reported in instrumental as well as historical catalogues (Pondrelli, 2002; Grünthal et al., 2013). Furthermore, there is significant coverage by geodetic instruments (Nocquet, 2012) – mostly the Global Positioning System (GPS) – to illuminate the kinematics of these tectonic units, as well as their temporal variations. In particular, the Apulia microplate is a candidate to test the hypothesis that microplates motions change in response to stress variations during the interseismic part of the earthquake cycle: in fact, the M_w 6.4 Durrës (Albania) earthquake stroke on 26 November 2019 along its eastern margin (Papadopoulos et al., 2020) (Fig. 1). This means that one can arrive at an estimate of the torque that has slowly built upon Apulia during the interseismic period on the basis of the focal mechanism and rupture area estimated for the 2019 Durrës earthquake. Furthermore, there is sufficient GPS coverage to infer with confidence past temporal variations of the Apulia rigid motion back to a decade or

so before the 2019 Durrës earthquake – that is, during the final years of the interseismic period. Here we utilise publicly-available records of GPS sites within Apulia to estimate a temporal change of the Euler vector describing its rigid motion during the periods from 2007/2008 to 2010, and from 2016/2017 to 2019 – that is, about a decade and immediately before the 2019 Durrës earthquake. Next, we estimate the torque needed to explain such a plate-motion temporal variation. Lastly, we compare it to a parameterised estimate of the torque arising from the stress buildup over the fraction of the 2019 Durrës earthquake cycle accomplished between 2007 and 2019.

2. Tectonics and kinematics of Apulia

The Apulia microplate (AP) comprises the southeastern part of Italy, and belongs to the tectonically complex region that buffers the convergence of Nubia towards Eurasia (e.g., Jolivet and Faccenna, 2000; Nocquet, 2012; Faccenna et al., 2014). Earlier studies (e.g., Anderson and Jackson, 1987) identified the northern and southern parts of Italy as one single tectonic unit named Adria. The existence of AP as a separate microplate in later tectonic models owes to the fact that several studies (Calais et al., 2002; Nocquet and Calais, 2002; Serpelloni et al., 2005; D'Agostino et al., 2008) concluded that a single rigid tectonic unit comprising the whole Adriatic Sea could not satisfy the kinematic constraints coming from a growing wealth of GPS observations collected in the region, and thus proposed the presence of two separate tectonic units – Adria to the north (e.g., Stein and Sella, 2005) and AP to the south. The microplate margin between Adria and AP cuts through the seismically active central Adriatic Sea (e.g., Weber et al., 2010) (Fig. 1). The western margin of AP runs along the Appennines, while to the east AP is bounded by the conjunction between the northern Albanides and the southern Dinarides. This is consistent with both GPS observations and earthquake slip vectors in the Apennines and the Dinarides (D'Agostino et al., 2008). Less clear is the location of the southern margin of Apulia, chiefly because of the absence of islands in the Ionian Sea where to deploy GPS devices that could measure local motions. Several previous studies (e.g., Battaglia et al., 2004; D'Agostino et al., 2008; Serpelloni et al., 2010) proposed a southern boundary of AP located between northern Calabria and southern Sicily. In a comprehensive review study of the contemporary kinematics of the Mediterranean, however, Nocquet (2012) noted that these proposals would imply an amount of relative motion between AP and the Ionian Sea that appears incompatible with the observed pattern of seismicity. Instead, here we place the southern margin of AP along the EW-directed South Salento–North Kerkira fault (Pierri et al., 2013), south of the Apulia-region southern coast (Fig. 1). We consider such a configuration to be reasonable on account that the southern margin of AP (i) runs through a cluster of regional seismicity in the northern Ionian Sea that is documented in both instrumental and historical seismic catalogues (Pondrelli, 2002; Grünthal et al., 2013), and (ii) coincides with an identified sliver of contemporary strike-slip deformation between the Adriatic and Ionian Seas (Kreemer et al., 2014).

The contemporary motion of AP can be inferred from a number of continuously-recording GPS sites whose data are publicly available for download at the Nevada Geodetic Laboratory website (Blewitt et al., 2018). While there are few publicly-available GPS continuous records until mid-2007, the number of continuously-recording instruments within AP whose data are publicly available has steadily grown from mid-2007 towards today. In fact, while prior to mid-2007 the number of GPS sites within AP is 5 or less, after then estimates of the AP motion can benefit from the availability of data from 10 to almost 20 GPS sites. We constrain the AP rigid motion over two distinct time periods that are 9 years apart from one another – that is, from November 2007 to October 2010, and from November 2016 to October 2019. The latter period is chosen so that it (i) is longer the 2.5 years that are commonly considered the minimum standard to obtain tectonically-representative velocities (e.g., Blewitt and Lavallée, 2002; Herring et al., 2018), and (ii) ends shortly before the 2019 Durrës earthquake. For the former period, we follow the same length criterion but request that – within the limits posed by the availability of GPS site records within AP – it begins as early as possible before the 2019 Durrës earthquake. Furthermore, in order to verify that the inferences and conclusions made here are not biased by the specific choice of initial/final time and period length, we constrain the AP rigid motion over three additional sets of time periods where the earlier and later ones are 9 years apart from one another – that is, January 2008–October 2010 versus January 2017–October 2019; July 2007–October 2010 versus July 2016–October 2019; and July 2007–June 2010 versus July 2016–June 2019. Such choices aim at constraining the AP rigid motion from the largest possible number of GPS sites over two $\sim$ 3-yr-long time periods (more precisely, they are 2.8 yr, 3 yr, and 3.3 yr long) that bound the longest possible fraction of the 2019 Durrës interseismic period permitted by the GPS data availability. In the following, we refer to, and present results for, the first set of time periods – that is, from November 2007 to October 2010 and from November 2016 to October 2019. Data and analyses for the other three sets of time periods are reported in the Supplementary Material. Given the constraints above, we select 8 sites for the earlier period (that going from 2007 to 2010), and 18 sites for the later period (that going from 2016 to 2019). These are illustrated in Fig. 1, while GPS-site acronyms and positions are reported in Tables 1 and 2. Fig. 2 schematically illustrates how these time periods fit within an idealised earthquake cycle assumed to end with the 2019 Durrës earthquake: the stress buildup $\Delta\sigma$ occurs over a period of time Δt_e that is in the order of few tens to few hundreds years (e.g., Stein and Wysession, 2003), and is followed by the sudden earthquake occurrence. The two $\sim$ 3-yr-long time periods over which we constrain the AP motion – from November 2007 to October 2010, and from November 2016 to October 2019 – are represented in Fig. 2 as Δt_{v1} and Δt_{v2}, respectively. Instead Δt_v represent the period from November 2007 to October 2019. In our analyses, Δt_e and $\Delta\sigma$ remain free parameters of the problem. The fraction of $\Delta\sigma$ accrued from the beginning of Δt_{v1} to the end of Δt_{v2} depends on these free parameters, and is equal to $\Delta\sigma \cdot \Delta t_v / \Delta t_e$. We process the continuous position time series of the sites in Fig. 1 using the MIDAS software (Blewitt et al., 2016), in order to obtain surface velocities and associated standard deviations that are representative of the GPS-site motions, in a reference frame fixed with the Eurasia plate (EU) (Kreemer et al., 2014), over the periods indicated above. Site velocities and associated standard deviations for earlier and later

Table 1
Continuous GPS stations utilised to constrain the AP Euler vector for the period November 2007–October 2010. Columns are: (1) sites acronyms, (2–3) longitude (decimal deg East) and latitude (decimal deg North) of site locations, (4–5) starting/ending time of GPS measurements (in decimal years), and (6–9) station East/North velocities (v_e/v_n) relative to Eurasia and standard deviations (σ) in mm/yr.

GPS stations			Temporal coverage		GPS velocities			
Site	lon	lat	Start	End	v_e	v_n	σ_{v_e}	σ_{v_n}
AMUR	16.604	40.907	2007.83	2010.83	1.1	5.4	0.3	0.3
CADM	16.274	41.078	2007.83	2010.83	1.7	5.3	0.4	0.4
GIUR	18.430	40.124	2007.83	2010.83	1.8	4.3	0.4	0.4
MRVN	16.196	41.061	2007.87	2010.83	1.2	5.4	0.4	0.3
NOCI	17.064	40.789	2007.83	2010.83	2.5	5.3	0.4	0.3
SASA	17.965	40.385	2007.83	2010.83	1.9	4.5	0.4	0.3
SCTE	18.467	40.072	2007.83	2010.83	1.2	4.6	0.3	0.3
UGEN	18.162	39.928	2007.83	2010.83	1.9	4.7	0.3	0.4

Table 2
Same as Table 1, but for the period November 2016–October 2019. GPS stations marked with a star (*) have also been used in the *similar-sites cases* (see main text for more details).

GPS stations			Temporal coverage		GPS velocities			
Site	lon	lat	Start	End	v_e	v_n	σ_{v_e}	σ_{v_n}
AMUR*	16.604	40.907	2016.84	2019.83	1.3	4.5	0.3	0.4
AVTR	17.733	40.342	2016.84	2019.50	0.9	4.4	0.4	0.4
BRIN	17.940	40.637	2016.84	2019.50	1.3	4.6	0.3	0.4
CSSR	18.347	39.833	2016.84	2019.83	0.5	4.4	0.3	0.3
FASA	17.359	40.835	2016.84	2019.83	1.1	4.5	0.3	0.3
GIUR*	18.430	40.124	2016.84	2019.83	0.8	4.3	0.3	0.4
MATG	16.705	40.649	2016.84	2019.83	1.3	4.6	0.3	0.4
MELE	18.335	40.278	2016.84	2019.50	0.9	4.1	0.3	0.4
MLFT	16.604	41.196	2016.84	2019.50	1.3	4.1	0.4	0.4
MRGH	16.149	41.373	2016.84	2019.83	1.2	4.6	0.3	0.3
MRVN*	16.196	41.061	2016.84	2019.39	1.0	4.1	0.4	0.4
MSAG	15.910	41.712	2016.84	2019.83	1.2	4.6	0.4	0.4
PATU	18.342	39.839	2016.84	2019.50	0.7	4.1	0.3	0.4
SASA*	17.965	40.385	2016.84	2019.83	1.0	4.3	0.3	0.3
SCTE*	18.467	40.072	2016.84	2019.83	0.7	4.1	0.3	0.3
UGEN*	18.162	39.928	2016.84	2019.83	1.0	4.1	0.3	0.3
USAL	18.111	40.335	2016.84	2019.83	0.3	3.8	0.4	0.4
VAL4	16.905	41.016	2016.84	2019.83	1.1	4.2	0.3	0.4

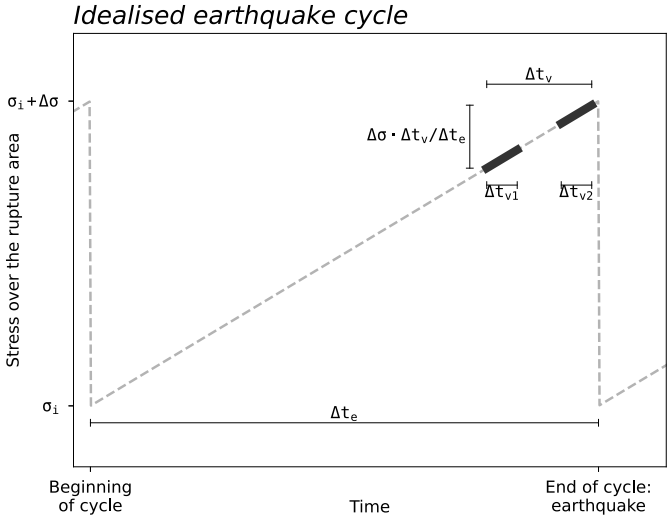

Fig. 2. Sketch of an idealised earthquake cycle illustrating how stress (vertical axis) slowly increases over time (horizontal axis) by $\Delta\sigma$ during the interseismic period, to then drop suddenly during the earthquake. The pattern of interseismic stress buildup and coseismic stress drop lasts Δt_e. Under the premise that the end of the idealised cycle represents the occurrence of the 2019 Durrës earthquake, the sketch also illustrates how the two time periods over which the GPS-based motion of Apulia is constrained (indicated as Δt_{v1} and Δt_{v2}) fit into such a cycle, bounding its last ~ 10 years (indicated as Δt_v).

periods are illustrated in Fig. 1, while velocity values are reported in Tables 1 and 2.

Next, we utilise the commonly-used minimisation of the sum of squared velocity misfits (Nocquet et al., 2001), to obtain from each set of site velocities an Euler vector that is representative of the AP/EU rigid motion during the associated time period. Specifically, for each period we draw 10^6 samples of each site velocity from their mean values and standard deviations. This provides us with 10^6 sets of site velocities, from which we infer an ensemble of 10^6 Euler vectors. From each ensemble we calculate mean Euler vectors and covariances of their Cartesian components. Lastly, for the later time period of each set, we also calculate an additional Euler vector through the same procedure above, but using data from only 6 GPS stations whose position time series also cover the earlier time period (see Table 2). This serves the purpose of testing whether a temporal change of Euler vector is warranted by the data also

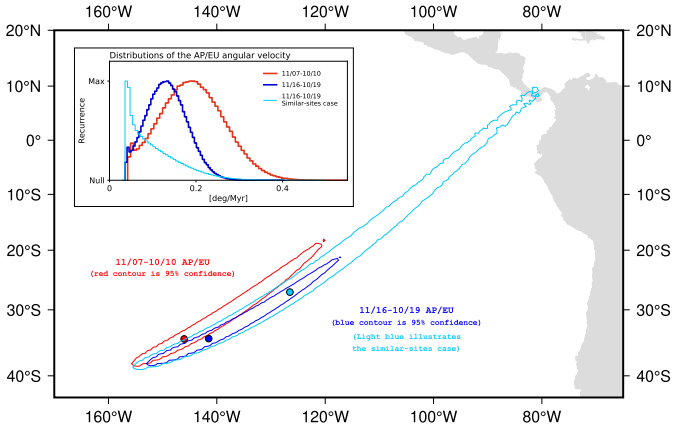

Fig. 3. Euler vectors for the motion of AP relative to EU inferred from the inversion of the AP GPS velocities (Fig. 1) via minimisation of the sum of squared misfits. The map shows the positions of the average Euler poles inferred for the two time periods, together with the contour where the most-recurrent 95% of the sampled Euler poles fall (see main text for details). Continents (in grey) are for reference. The inset shows the distributions of sampled angular velocities associated with the Euler poles.

under more stringent conditions that are as similar as possible over the two time periods. In the following, inferences drawn from having used the latter Euler vector over the later time period (as opposed to the one making use of the entire group of available stations – see Table 2) are labeled as *similar-sites case*. Table 3 reports all calculated Euler vectors (including those for the additional three sets of time periods), along with the entries of their covariance matrices. Fig. 3 shows position and confidence area of the inferred Euler poles, as well as the distributions of angular velocities within the ensembles. The temporal change of AP/EU Euler vector concerns both the angular velocity, whose mean value almost halves from one period to the other, and the Euler pole, which shifts by ~ 100 km eastward. From the AP/EU Euler vectors ($\vec{\omega}$) we first calculate surface velocities at the positions of the GPS sites (that is, $\vec{v}_P = \vec{\omega} \times \vec{r}$, $\vec{r}$ being the site position vector), and then calculate residual velocities ($\vec{v}_R$) as the difference between the GPS observed velocity ($\vec{v}_O$) and its prediction from the Euler vectors at the site – that is, $\vec{v}_R = \vec{v}_O - (\vec{\omega} \times \vec{r})$. Fig. 4 shows residual velocities for both periods for all sites (values are reported in Supplementary Tables 1 and 2). The fact that velocity residuals are smaller than their uncertainties means that the velocity fields measured by GPS instruments over both periods are in fact adequately described by Euler vectors – that is, they are velocity fields that represent rigid motions over the Earth's surface.

We use the inferred Euler vectors and associated covariances to sample on a regularly-spaced grid the AP surface motions and 95% confidence regions, where the most-recurrent 95% of the ensemble of 10^6 velocity samples fall (Fig. 5). This shows that the motion of AP decreased by $\sim 20\%$, from velocities in range from 5 to 5.5 mm/yr between November 2007 and October 2010, to velocities in range from 4 to 4.5 mm/yr between November 2016 and October 2019. Simultaneously to the slowdown, the direction of motion turned overall westward by $\sim 10°$. Importantly, these kinematic variations are larger than the 95% confidence range associated with the Euler vectors covariances. The fact that the AP rigid-motion change is larger than what is permitted by the combined uncertainties of both Euler vectors means that such a decadal kinematic change is warranted by the data at the 95% confidence level, and shall be viewed as a tectonically-meaningful plate-motion change. To further corroborate this inference, we performed an F-ratio test (Stein and Gordon, 1984) to calculate the residual probability that GPS station velocities of both the earlier and later time periods can be efficiently described by one single

Table 3
Euler vectors ($\vec{\omega}$) and associated covariances (C_{ij}) for the AP/EU rigid motions during all time periods investigated in this study. Labels for earlier/later time periods are: E1 (11/07–10/10), E2 (01/08–10/10), E3 (07/07–06/10), E4 (07/07–10/10), L1 (11/16–10/19), L2 (01/17–10/19), L3 (07/16–06/19), L4 (07/16–10/19). Euler vectors whose time period is marked with a star (*) refer to the *similar-sites cases* (see main text for more details).

	lon	lat	ω	ω_x	ω_y	ω_z	C_{xx}	C_{xy}	C_{xz}	C_{yy}	C_{yz}	C_{zz}
	[° E]	[° N]	[° Myr^{-1}]	[10^{-2} ° Myr^{-1}]			[10^{-8} rad^2 Myr^{-2}]					
E1	-146.03	-34.58	0.190	-12.95	-8.72	-10.76	99.1	31.1	88.1	9.8	27.6	78.4
E2	-147.84	-35.23	0.212	-14.64	-9.21	-12.21	105.5	33.1	93.8	10.4	29.5	83.5
E3	-133.87	-28.22	0.105	-7.57	-6.99	-5.94	112.9	35.4	100.4	11.2	31.5	89.4
E4	-141.57	-32.85	0.147	-9.90	-7.71	-8.13	89.8	28.2	79.9	8.9	25.1	71.1
L1	-141.51	-34.51	0.131	-8.45	-6.72	-7.42	41.5	13.1	37.0	4.2	11.7	33.0
L2	-139.67	-34.25	0.119	-7.52	-6.39	-6.72	45.2	14.3	40.6	4.5	12.84	36.4
L3	-139.77	-33.38	0.122	-7.75	-6.55	-6.69	42.7	13.6	38.1	4.3	12.1	34.0
L4	-142.42	-34.50	0.140	-9.12	-7.02	-7.91	37.7	12.0	33.6	3.8	10.7	30.0
L1*	-126.51	-27.12	0.073	-3.89	-5.25	-3.35	144.5	46.3	128.1	14.9	41.1	113.7
L2*	-111.09	-17.39	0.051	-1.75	-4.53	-1.52	163.9	52.5	145.4	16.9	46.6	129.0
L3*	-138.18	-32.33	0.113	-7.14	-6.40	-6.07	134.6	43.2	119.4	13.9	38.3	106.0
L4*	-139.33	-33.07	0.120	-7.62	-6.55	-6.54	125.1	40.2	111.0	12.9	35.6	98.5

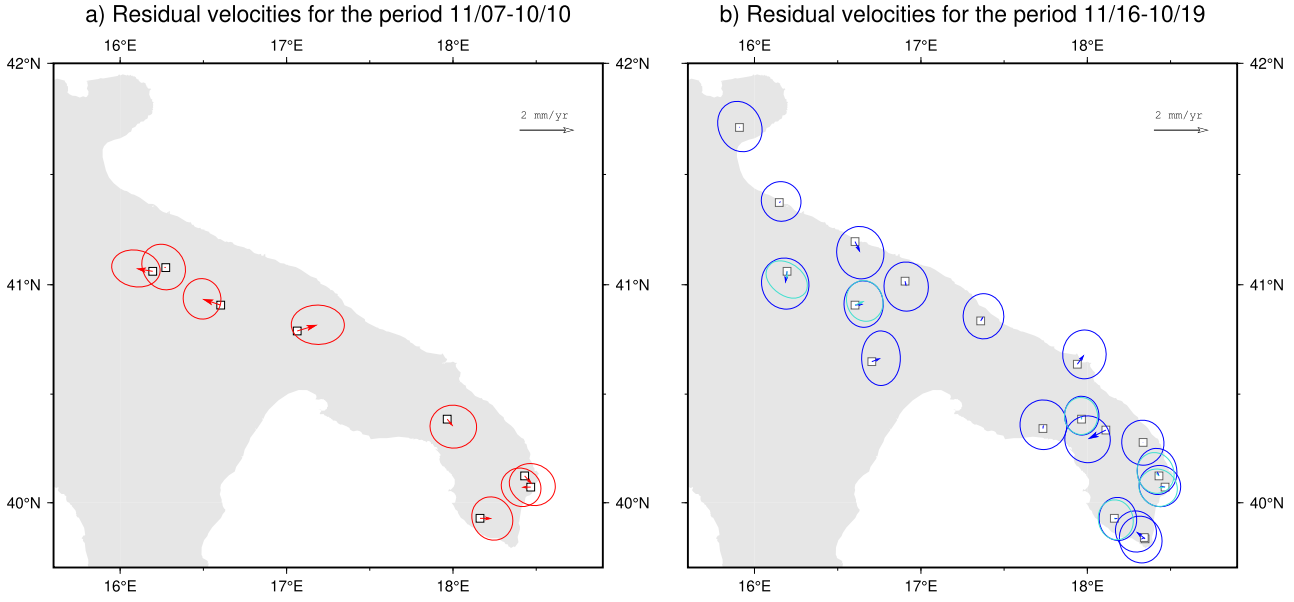

Fig. 4. (a) Surface velocity residuals (see main text for details on calculation) of GPS sites utilised to infer the AP/EU Euler vector for the period from November 2007 to October 2010. Ellipses are 95% confidence. (b) Same as (a), but for the GPS sites utilised to infer the AP/EU Euler vector for the period from November 2016 to October 2019. In light blue are residuals from the similar-sites case (see main text for details).

AP/EU Euler vector – that is, we assess the level of confidence one can have in stating that the Euler vector has not changed through time. We find that there is less than 0.2% probability that such a statement is true based on the observed GPS velocities, regardless of the set of earlier/later time periods or the number of GPS stations utilised for inferring the AP/EU Euler vector over the later period (i.e., whether or not one refers to the similar-site case). Under such a premise, it is difficult to imagine geological processes capable of generating tectonically-adequate levels of stress over years to decades, other than the earthquake cycle. Furthermore, the observed slowdown of the AP/EU motion appears consistent with the stress buildup during the Durrës interseismic period, which can be constrained from the characteristics of the earthquake mechanism of the 2019 Durrës event. In fact, the latter event has been identified to be the result of thrust faulting occurring on a Northwest–Southeast striking reverse fault (Govorčin et al., 2020) on the eastern margin of AP (Fig. 1). As such, the stress that EU exerted upon AP during the interseismic period preceding the 2019 Durrës earthquake must have been oriented roughly Northeast–Southwest, which indeed coincides with the direction of AP slowdown implied by its Euler-vector temporal change (Fig. 5).

3. Torque variations upon Apulia

The considerations above motivate us to explore quantitatively whether the AP observed plate-motion change accomplished from 2007 to 2019 is the result of the interseismic stress buildup, over the same period, that preceded the 2019 Durrës earthquake. In order to test such a hypothesis, we estimate the torque variation experienced by AP as a result of the interseismic stress buildup from 2007 to 2019, and compare it with estimates of the torque variation required upon AP in order to change its Euler vector to the degree evidenced by the geodetic data.

3.1. Torque variation required upon AP

For the latter torque variation, we resort to previous studies (Iaffaldano and Bunge, 2015; Martin de Blas and Iaffaldano, 2019) that obtained an analytical equation linking the torque variation $\Delta\vec{M}$ experienced by a tectonic plate of basal area S to the resulting temporal change of Euler vector. If one writes two equations expressing the torque balance of a tectonic plate at two distinct points in time – t_1 and t_2 – and then takes the difference between

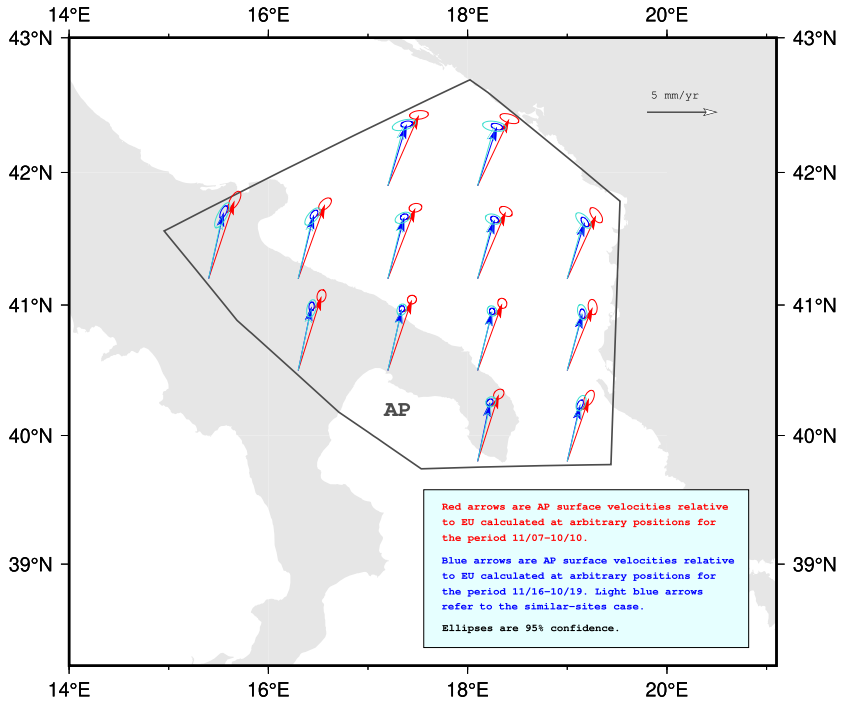

Fig. 5. Surface velocities illustrating the motion of AP relative to EU over the two time periods for which Euler vectors are inferred. Velocities are calculated at evenly-spaced positions within AP. Contours around velocity arrows are the 95% confidence regions on velocities. AP margins are in thick black. Continents are in grey.

them so that only the terms that have actually changed through time remain in the resulting equation, one obtains

$$\Delta\vec{M} = \int_S \frac{\mu_A}{H_A} \cdot \vec{r} \times [\vec{v}_p(\vec{r}, t_2) - \vec{v}_p(\vec{r}, t_1)] \cdot dS \tag{1}$$

where μ_A and H_A are viscosity and thickness of the asthenosphere, while $\vec{v}_p(\vec{r}, t)$ is the plate motion at position $\vec{r}$ and time t (see Iaffaldano and Bunge, 2015; Martin de Blas and Iaffaldano, 2019, for more details and equation development). Since $\vec{v}_p(\vec{r}, t) = \vec{\omega}(t) \times \vec{r}$, equation (1) becomes

$$\Delta\vec{M} = \int_S \frac{\mu_A}{H_A} \cdot \vec{r} \times [\Delta\vec{\omega} \times \vec{r}] \cdot dS \tag{2}$$

where $\Delta\vec{\omega} = \vec{\omega}(t_2) - \vec{\omega}(t_1)$. The fact that the Euler-vector change $\Delta\vec{\omega}$ is independent of $\vec{r}$ means that the integral may be written as the result of a linear map

$$\int_S \frac{\mu_A}{H_A} \cdot \vec{r} \times [\Delta\vec{\omega} \times \vec{r}] \cdot dS = \underbrace{\begin{pmatrix} \int_S \frac{\mu_A}{H_A}(y^2+z^2)dS & -\int_S \frac{\mu_A}{H_A}xydS & -\int_S \frac{\mu_A}{H_A}xzdS \\ -\int_S \frac{\mu_A}{H_A}xydS & \int_S \frac{\mu_A}{H_A}(x^2+z^2)dS & -\int_S \frac{\mu_A}{H_A}yzdS \\ -\int_S \frac{\mu_A}{H_A}xzdS & -\int_S \frac{\mu_A}{H_A}yzdS & \int_S \frac{\mu_A}{H_A}(x^2+y^2)dS \end{pmatrix}}_{\mathbf{P}} \times \begin{pmatrix} \Delta\omega_x \\ \Delta\omega_y \\ \Delta\omega_z \end{pmatrix} \tag{3}$$

where the operator $\mathbf{P}$ links the vectorial space of Euler-vector changes that a tectonic plate could experience to that of torque variations possibly acting upon it. Therefore,

$$\Delta\vec{M} = \mathbf{P}\Delta\vec{\omega} \tag{4}$$

Equation (4) holds when the time periods over which $\Delta\vec{M}$ and $\Delta\vec{\omega}$ are accomplished are (i) short enough (in a geological sense) that the plate has not changed shape, but also (ii) long enough that the elastic component of sublithospheric motion within the viscoelastic asthenosphere – which affects velocities of the overlying plate (e.g., Pollitz et al., 2006) – has decayed to a significant extent. These conditions indeed apply to AP for Euler vectors calculated using GPS data collected between 2007 and 2010, and between 2016 and 2019, since these two periods are more than 2–3 Maxwell time-intervals apart from each other (see Supplementary Material for calculation of the Maxwell time-interval of the asthenosphere underneath AP). We draw 10^6 samples of the two AP Euler vectors inferred above, and use them to build ensembles of geodetically-constrained AP Euler-vector changes that we then map, through equation (4), into ensembles of torque variations needed to generate the AP temporal change of rigid motion. In doing so, we implement the findings of previous studies of long-wavelength glacial rebound data (Paulson and Richards, 2009; Richards and Lenardic, 2018), which constrain the cube of the asthenosphere thickness to be proportional to the viscosity contrast between the asthenosphere and the upper mantle – i.e., $H_A^3 = a \cdot (\mu_A/\mu_M)$, with $a = 4.67 \cdot 10^5$ km^3 (see Fig. 3 in Richards and Lenardic, 2018). Assuming the global average of μ_A is $5 \cdot 10^{19}$ Pa·s and that of μ_M is $1.5 \cdot 10^{21}$ Pa·s yields $H_A \sim 150$ km. Instead, $H_A \sim 130$ km if the global average of μ_A is assumed to be $3 \cdot 10^{19}$ Pa·s. In addition, we also implement asthenosphere lateral variations of viscosity in line with the lateral temperature variations mapped by the tomography model `PM_v2_2012` by Priestley and McKenzie (2013) (see Supplementary Material for details and images). Table 4 reports the obtained entries of the AP-specific operator $\mathbf{P}$ when the viscosity of the upper mantle is set to $1.5 \cdot 10^{21}$ Pa·s and μ_A is set variably to $3 \cdot 10^{19}$ and $5 \cdot 10^{19}$ Pa·s (e.g., Fjeldskaar, 1994; Mitrovica and Forte, 2004).

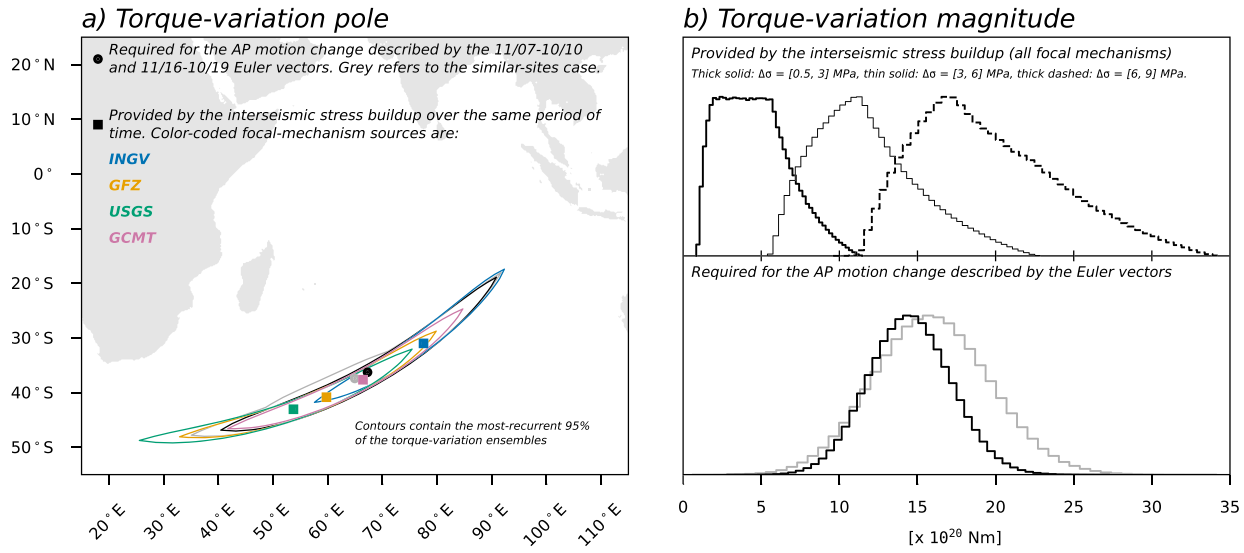

Fig. 6. Comparison of torque variation required upon AP in order to generate the plate-motion change evidenced by GPS data, and torque variation provided to AP by the interseismic stress buildup of the Durrës earthquake cycle between November 2007 and October 2019. Torque-variation poles (i.e., the geographical positions where the torque-variation axes intersect Earth's surface) and their 95% confidence regions are shown in (a). Distributions of the associated torque-variation magnitudes are in (b). The coseismic stress drop $\Delta\sigma$, the average asthenosphere viscosity μ_A, the length of the 2019 Durrës earthquake cycle Δt_e, and the size of the rupture area Σ_e are free parameters of the calculations (see main text for details). For $\Delta\sigma$, three ranges in line with global earthquake statistics (see legend in panel b) are utilised. $\mu_A = 5 \cdot 10^{19}$ Pa·s, Δt_e is uniformly distributed in range from 50 to 150 years, and $\Sigma_e = 250$ km^2. In the Supplementary Material, similar comparisons featuring different values of the controlling parameters are shown.

Table 4
Entries of the linear operator **P** in equation (4). Units are 10^{37} Pa · s · m^3.

μ_A	$\mathbf{P}_{11}$	$\mathbf{P}_{12}$	$\mathbf{P}_{13}$	$\mathbf{P}_{22}$	$\mathbf{P}_{23}$	$\mathbf{P}_{33}$
$3 \cdot 10^{19}$ Pa · s	6.8	-2.3	-6.6	13.3	-2.1	7.9
$5 \cdot 10^{19}$ Pa · s	13.9	-4.7	-13.5	27.1	-4.3	16.2

3.2. Torque variation from the Durrës interseismic stress buildup between November 2007 and October 2019

We proceed under the premise that the stress buildup during the entire interseismic period is equal in magnitude but opposite in direction to the sudden coseismic stress associated with the occurrence of the 2019 Durrës earthquake. The direction of the latter one – here indicated with the unit-vector symbol $\hat{s}$ – can be determined from the strike, dip, and rake of the main nodal plane, while its magnitude $\Delta\sigma$ is kept as a free parameter. Thus, the torque variation $\Delta\vec{M}_e$ exerted by the 2019 Durrës earthquake upon AP may be parameterised as

$$\Delta\vec{M}_e = (\Delta\sigma \cdot \Sigma_e) \cdot [\vec{r}_e \times \hat{s}] \tag{5}$$

where $\vec{r}_e$ is the position of the earthquake hypocenter, while Σ_e is the size of the rupture area. Accordingly, the torque variation $\Delta\vec{M}_i$ experienced by AP during the fraction of interseismic period equal to the time period bounded by the two GPS-derived Euler vectors (Δt_v in Fig. 2) can be expressed as

$$\Delta\vec{M}_i = -1 \cdot \frac{\Delta t_v}{\Delta t_e}\Delta\vec{M}_e = -1 \cdot \frac{\Delta t_v}{\Delta t_e} \cdot (\Delta\sigma \cdot \Sigma_e) \cdot [\vec{r}_e \times \hat{s}] \tag{6}$$

where the negative sign accounts for the fact that the stress during the interseismic period acts in a direction opposite to that of the sudden coseismic stress, while the coefficient $\Delta t_v/\Delta t_e$ is the fraction of interseismic period corresponding to the period between November 2007 and October 2019.

We constrain the unit vector $\hat{s}$ from four independent focal mechanism solutions – i.e., strike, dip, and rake – provided by the USGS, the INGV, the GFZ, and the GCMT repository. We elect to assume an uncertainty on each of the parameters equal to 7°. Previous studies (Caporali et al., 2020; Ganas et al., 2020; Papadopoulos et al., 2020; Vittori et al., 2020; Panuntun, 2021) constrained the size of the rupture area Σ_e in range from 250 to 350 km^2, and its lateral extent to be around 20 km. Thus, assuming an uncertainty of 7° on the focal mechanism strike is equivalent to assuming an uncertainty of about 1 km on the location of the surface projection of the rupturing-fault lateral extent. Furthermore, we perform calculations taking the stress drop $\Delta\sigma$ variably in range from 0.1 to 3 MPa, from 3 to 6 MPa, and from 6 to 9 MPa (e.g., Allmann and Shearer, 2009). Lastly, since the length of the interseismic period Δt_e of the 2019 Durrës earthquake is not known, we take it in a deliberately wide range from 50 to 150 years, which is nonetheless in line with previous studies on earthquake recurrence (e.g., Saichev and Sornette, 2007; Zöller et al., 2007). For each focal mechanism solution, we draw 10^6 samples of these parameters from uniform distributions within the ranges indicated above. From these, we generate 10^6 samples of parameter sets and build an ensemble of 10^6 realisations of $\Delta\vec{M}_i$. In building these ensembles, we keep the value of Σ_e constant and equal to, variably, the end-members of the rupture-area range above.

4. Discussion

In Fig. 6 we compare the torque variations required upon AP ($\Delta\vec{M}$) and provided by the November 2007–October 2019 interseismic stress buildup ($\Delta\vec{M}_i$). Specifically, in Fig. 6a we compare the directions of the torque-variation vectors by looking at their pole locations, where the torque-variation axes – i.e., axes directed as $\Delta\vec{M}/|\Delta\vec{M}|$ and $\Delta\vec{M}_i/|\Delta\vec{M}_i|$ – intersect the Earth's surface. Instead, in Fig. 6b we compare the distributions of magnitude of torque variations from the ensembles generated above. The three distributions of magnitude of $\Delta\vec{M}_i$ refer to three different ranges of assumed stress drop $\Delta\sigma$: from 0.5 to 3 MPa (in thick solid), from 3 to 6 MPa (in thin solid), and from 6 to 9 MPa (in thick dashed). In Fig. 6 the ensemble of $\Delta\vec{M}$ features an average viscosity of the asthenosphere $\mu_A = 5 \cdot 10^{19}$ Pa · s, while the ensemble of $\Delta\vec{M}_i$ features $\Sigma_e = 250$ km^2. In the Supplementary Material we show similar figures, but for ensembles featuring $\mu_A = 3 \cdot 10^{19}$ Pa·s and $\Sigma_e = 350$ km^2. We find that the ensemble of torque varia-

tions required to explain the AP rigid motion change is in agreement with that of the torque variations generated upon AP by the November 2007–October 2019 interseismic stress buildup. In fact, the regions where the most recurrent 95% of the ensembles poles fall do overlap to a large extent (Fig. 6a). This means that the force required upon AP to slow down its motion between November 2007 and October 2019 is oriented in line with the direction of interseismic stress buildup over the same period. The distributions of magnitude of $\Delta\vec{M}$ and $\Delta\vec{M}_i$ are also consistent with each other, indicating that enough interseismic stress has been built up over the same period to impact onto the AP rigid motion and change it to the degree evidenced by GPS data. The Supplementary Material reports the same comparisons, but for Euler vectors and associated torque variations obtained using GPS stations velocities for the three additional sets of time periods – that is, January 2008–October 2010 versus January 2017–October 2019; July 2007–October 2010 versus July 2016–October 2019; and July 2007–June 2010 versus July 2016–June 2019. The agreement between torque variations required upon AP and provided by the interseismic stress buildup overall holds also in these cases. Furthermore, the overlap between torque-variation magnitude distributions occurs despite the uncertainty associated with not knowing precise values of asthenosphere average viscosity, the length of the 2019 Durrës earthquake cycle, the size of its rupture area, or its coseismic stress drop (see also figures in the Supplementary Material). In other words, the inference that the torque variation generated upon AP by the interseismic stress buildup between 2007/2008 and 2019 is in agreement with what is needed to generate the observed change of AP rigid motion over the same period holds despite the trade-offs between the parameters above, which torque-variation calculations are inevitably subject to. These results indicate the existence of whole-AP kinematic changes associated with the stress cycle of a relatively large earthquake occurring along its margins, and call for investigating whether similar dynamics take place in other tectonic settings characterised by the presence of microplates or small-/medium-sized plates.

5. Conclusions

We inferred Euler vectors describing the rigid motion of the Apulia microplate over the periods from 2007/2008 to 2010, and from 2016/2017 to 2019 from publicly-available, continuous GPS time series collected at sites within Apulia. These data, which constrain the Apulia rigid motion over a decade preceding the M_W 6.4, 26 November 2019 Durrës earthquake, evidence a $\sim$ 20% slowdown and $\sim 10^\circ$ westward turn of the microplate motion that exceed what is permitted by data uncertainties, and are thus representative of a tectonically-meaningful kinematic change. We estimated the torque variation required upon the Apulia microplate in order to generate the GPS-constrained motion change, and find that it is in agreement with parameterised estimates of the torque variation imparted to the Apulia microplate by the Durrës interseismic stress buildup occurred between 2007 and 2019, prior to the Durrës earthquake. The agreement holds for values of the controlling parameters (asthenosphere average viscosity, length of the 2019 Durrës earthquake cycle, size of its rupture area, and its coseismic stress drop) within realistic ranges. On this basis, we conclude that the interseismic stress buildup preceding the 2019 Durrës earthquake influenced the Apulia microplate motion in a measurable way.

CRediT authorship contribution statement

Giampiero Iaffaldano: Conceptualization, Formal analysis, Investigation, Software, Supervision, Validation, Writing – original draft, Writing – review & editing. **Juan Martin de Blas:** Formal analysis, Investigation, Software, Validation, Writing – review & editing. **Bjartur Í Dali Udbø:** Formal analysis, Investigation, Validation.

Declaration of competing interest

The authors declare that they have no known competing financial interests or personal relationships that could have appeared to influence the work reported in this paper.

Data and materials availability

All data and software used in this study are referenced within the main text or the figure captions. Some of the figures were generated using the Generic Mapping Tools (Wessel et al., 2019). Focal mechanism solutions used in this study are available at the following repositories:

USGS – earthquake.usgs.gov/earthquakes/eventpage/us70006d0m/moment-tensor
INGV – cnt.rm.ingv.it/en/event/23487611/?tab=MeccanismoFocale
GFZ – geofon.gfz-potsdam.de/old/data/alerts/2019/gfz2019xdig/mt.txt
GCMT – www.globalcmt.org/CMTsearch.html.

Acknowledgements

Authors are grateful to the editor, Rebecca Bendick, and two anonymous reviewers for careful comments that improved the manuscript. GI acknowledges support by a research grant (00023121) from Villum Fonden. JMB acknowledges support from a fellowship (LCF/BQ/EU17/11590058) from La Caixa banking foundation (ID 100010434), as well as support from the Department of Geosciences and Natural Resource Management at the University of Copenhagen.

Appendix A. Supplementary material

Supplementary material related to this article can be found online at https://doi.org/10.1016/j.epsl.2022.117505.

References

Allmann, B., Shearer, P., 2009. Global variations of stress drop for moderate to large earthquakes. J. Geophys. Res. 114, B01310.
Anderson, H., Jackson, J., 1987. Active tectonics of the Adriatic region. Geophys. J. R. Astron. Soc. 91, 937–983.
Battaglia, M., Murray, M.H., Serpelloni, E., Bürgmann, R., 2004. The Adriatic region: an independent microplate within the Africa-Eurasia collision zone. Geophys. Res. Lett. 31 (9), 587–610.
Blewitt, G., Hammond, W., Kreemer, C., 2018. Harnessing the GPS data explosion for interdisciplinary science. Eos 99.
Blewitt, G., Kreemer, C., Hammond, W., Gazeaux, J., 2016. MIDAS robust trend estimator for accurate GPS station velocities without step detection. J. Geophys. Res. 121, 2054–2068.
Blewitt, G., Lavallée, D., 2002. Effect of annual signals on geodetic velocity. J. Geophys. Res. 107 (B7), 2145.
Calais, E., Nocquet, J.M., Jouanne, F., Tardy, M., 2002. Current strain regime in the Western Alps from continuous Global Positioning System measurements, 1996–2001. Geology 30, 651–654.
Caporali, A., Floris, M., Chen, X., Nurce, B., Bertocco, M., Zurutuza, J., 2020. The November 2019 seismic sequence in Albania: geodetic constraints and fault interaction. Remote Sens. 12, 846.
D'Agostino, N., Avallone, A., Cheloni, D., D'Anastasio, E., Mantenuto, S., Selvaggi, G., 2008. Active tectonics of the Adriatic region from GPS and earthquake slip vectors. J. Geophys. Res., Solid Earth 113 (B12).
Faccenna, C., Becker, T.W., Auer, L., Billi, A., Boschi, L., Brun, J.-P., Capitanio, F.A., Funiciello, F., Horvath, F., Jolivet, L., Piromallo, C., Royden, L., Rossetti, F., Serpelloni, E., 2014. Mantle dynamics in the Mediterranean. Rev. Geophys. 52, 283–332.
Fjeldskaar, W., 1994. Viscosity and thickness of the asthenosphere detected from the Fennoscandian uplift. Earth Planet. Sci. Lett. 126, 399–410.

Ganas, A., Elias, P., Briole, P., Cannavo, F., Valkaniotis, S., Tsironi, V., Partheniou, E.I., 2020. Ground deformation and seismic fault model of the M6.4 Durrës (Albania) Nov. 26, 2019 earthquake, based on GNSS/INSAR observations. Geosciences 10 (6).
Govers, R., Furlong, K., van de Wiel, L., Herman, M., Broerse, T., 2018. The geodetic signature of the earthquake cycle at subduction zones: model constraints on the deep processes. Rev. Geophys. 56, 6–49.
Govorčin, M., Wdowinski, S., Matoš, B., Funning, J., 2020. Geodetic source modeling of the 2019 Mw 6.3 Durrës, Albania, earthquake: partial rupture of a blind reverse fault. Geophys. Res. Lett. 47, e2020GL088990.
Grünthal, G., Wahlström, R., Stromeyer, D., 2013. The SHARE European Earthquake Catalogue (SHEEC) for the time period 1900–2006 and its comparison to the European-Mediterranean Earthquake Catalogue (EMEC). J. Seismol. 17, 1339–1344.
Herring, T.A., King, R.W., Floyd, M.A., McClusky, S.C., 2018. Introduction to GAMIT/GLOBK. Release 10.7, Massachusetts Institute of Technology, Cambridge.
Iaffaldano, G., 2014. A geodynamical view on the steadiness of geodetically-derived rigid plate-motions over geological time. Geochem. Geophys. Geosyst. 15, 238–254.
Iaffaldano, G., Bunge, H.-P., 2015. Rapid plate motion variations: observations serving geodynamic interpretation. Annu. Rev. Earth Planet. Sci. 43, 571–592.
Jolivet, L., Faccenna, C., 2000. Mediterranean extension and the Africa-Eurasia collision. Tectonics 19, 1095–1106.
Kreemer, C., Blewitt, G., Klein, E., 2014. A geodetic plate motion and global strain rate model. Geochem. Geophys. Geosyst. 15, 3849–3889.
Le Pichon, X., 1968. Sea-floor spreading and continental drift. J. Geophys. Res. 73, 3661–3697.
Martin de Blas, J., Iaffaldano, G., 2019. Using rigid microplate motions to detect the stress buildup preceding large earthquakes: a feasibility test based on synthetic models. J. Geophys. Res., Solid Earth 124 (12), 13468–13485.
McKenzie, D.P., Parker, R.L., 1967. The North Pacific: an example of tectonics on a sphere. Nature 216, 1276–1280.
Mitrovica, J.X., Forte, A.M., 2004. A new inference on mantle viscosity based upon joint inversion of convection and glacial isostatic adjustment data. Earth Planet. Sci. Lett. 225, 177–189.
Morgan, W.J., 1968. Rises, trenches, great faults, and crustal blocks. J. Geophys. Res. 73, 1959–1982.
Nocquet, J.-M., 2012. Present-day kinematics of the Mediterranean: a comprehensive overview of GPS results. Tectonophysics 579, 220–242.
Nocquet, J.-M., Calais, E., 2002. Crustal velocity field of western Europe from permanent GPS array solutions, 1996–2001. Geophys. J. Int. 154, 72–88.
Nocquet, J.-M., Calais, E., Altamimi, Z., Sillard, P., Boucher, C., 2001. Intraplate deformation in western Europe deduced from an analysis of the International Terrestrial Reference Frame 1997 (ITRF97) velocity field. J. Geophys. Res. 106, 11239–11257.
Panuntun, H., 2021. Geodetic slip model of the November 26, 2019 Albania earthquake estimated from Sentinel-1 TOPS interferometry. Tectonophysics 807, 228814.
Papadopoulos, G.A., Agalos, A., Carydis, P., Lekkas, E., Mavroulis, S., Triantafyllou, I., 2020. The 26 November 2019 Mw 6.4 Albania destructive earthquake. Seismol. Res. Lett. 91 (6), 3129–3138.
Paulson, A., Richards, M.A., 2009. On the resolution of radial viscosity structure in modelling long-wavelength postglacial rebound data. Geophys. J. Int. 179, 1516–1526.
Pierri, P., de Lorenzo, S., Calcagnile, G., 2013. Analysis of the low-energy seismic activity in the Southern Apulia (Italy). Open J. Earthq. Res. 2 (4), 91–105.
Pollitz, F., Bürgmann, R., Banerjee, P., 2006. Post-seismic relaxation following the great 2004 Sumatra-Andaman earthquake on a compressible self-gravitating Earth. Geophys. J. Int. 167, 397–420.
Pondrelli, S., 2002. European-Mediterranean Regional Centroid-Moment Tensors Catalog (RCMT) [data set].
Priestley, K., McKenzie, D., 2013. The relationship between shear wave velocity, temperature, attenuation and viscosity in the shallow part of the mantle. Earth Planet. Sci. Lett. 381, 78–91.
Richards, M.A., Lenardic, A., 2018. The Cathles parameter (Ct): a geodynamic definition of the asthenosphere and implications for the nature of plate tectonics. Geochem. Geophys. Geosyst. 19 (12), 4858–4875.
Saichev, A., Sornette, D., 2007. Theory of earthquake recurrence times. J. Geophys. Res. 112, B04314.
Savage, J., 1983. A dislocation model of strain accumulation and release at a subduction zone. J. Geophys. Res. 88, 4984–4996.
Serpelloni, E., Anzidei, M., Baldi, P., Casula, G., Galvani, A., 2005. Crustal velocity and strain-rate fields in Italy and surrounding regions: new results from the analysis of permanent and non-permanent GPS networks. Geophys. J. Int. 161, 861–880.
Serpelloni, E., Bürgmann, R., Anzidei, M., Baldi, P., Ventura, B.M., Boschi, E., 2010. Strain accumulation across the Messina Straits and kinematics of Sicily and Calabria from GPS data and dislocation modeling. Earth Planet. Sci. Lett. 298, 347–360.
Stein, S., Gordon, R.G., 1984. Statistical tests of additional plate boundaries from plate motion inversions. Earth Planet. Sci. Lett. 69, 401–412.
Stein, S., Sella, G.F., 2005. Pleistocene Change from Convergence to Extension in the Apennines as a Consequence of Adria Microplate Motion. Springer, Netherlands, pp. 21–34.
Stein, S., Wysession, M., 2003. An Introduction to Seismology, Earthquakes, and Earth Structure. Blackwell Publishing.
Stotz, I.L., Iaffaldano, G., Davies, D.R., 2018. Pressure driven Poiseuille flow: a major component of the torque-balance governing Pacific Plate motion. Geophys. Res. Lett. 45, 117–125.
Vittori, E., Blumetti, A.M., Comerci, V., Di Manna, P., Piccardi, L., Gega, D., Hoxha, I., 2020. Geological effects and tectonic environment of the 26 November 2019, Mw 6.4 Durrës earthquake (Albania). Geophys. J. Int. 225 (2), 1174–1191.
Wallace, L.M., McCaffrey, R., Beavan, J., Ellis, S., 2005. Rapid microplate rotations and backarc rifting at the transition between collision and subduction. Geology 33, 857–860.
Weber, J., Vrabec, M., Pavlovčič-Prešeren, P., Dixon, T., Jiang, Y., Stopar, B., 2010. GPS-derived motion of the Adriatic microplate from Istria Peninsula and Po Plain sites, and geodynamic implications. Tectonophysics 283, 214–222.
Wessel, P., Luis, J.F., Uieda, L., Scharroo, R., Wobbe, F., Smith, W.H.F., Tian, D., 2019. The generic mapping tools version 6. Geochem. Geophys. Geosyst. 20 (11), 5556–5564.
Wilson, J.T., 1965. A new class of faults and their bearing on continental drift. Nature 207, 343–347.
Zöller, G., Ben-Zion, Y., Holschneider, M., Hainzl, S., 2007. Estimating recurrence times and seismic hazard of large earthquakes on an individual fault. Geophys. J. Int. 170, 1300–1310.